# A large area CCD X-ray detector for exotic atom spectroscopy

N. Nelms[a],*, D.F. Anagnostopoulos[b], O. Ayranov[c,1], G. Borchert[d], J.-P. Egger[e],
D. Gotta[d], M. Hennebach[d], P. Indelicato[f], B. Leoni[c], Y.W. Liu[c], B. Manil[f],
L.M. Simons[c], A. Wells[a]

[a] *Department of Physics and Astronomy, Space Research Centre, University of Leicester, Leicester LE1 7RH, UK*
[b] *University of Ioannina, Department Materials Science and Technology, Ioannina, Greece*
[c] *Paul Scherrer-Institut (PSI), Villigen, Switzerland*
[d] *Institut für Kernphysik, Forschungszentrum Jülich, Germany*
[e] *Institut de Physique de L'Université de Neuchâtel, Switzerland*
[f] *Université Pierre et Marie Curie, Laboratoire Kastler-Brossel, F-75252 Paris, France*

## Abstract

A large area, position and energy sensitive detector has been developed to study the characteristic X-radiation of exotic atoms in the few keV range. The detector, built up from an array of six high-resistivity CCDs, is used as the focal plane of a reflection-type crystal spectrometer. A large detection area is necessary because of the need to detect simultaneously two or more lines close in energy as well as broad structures like fluorescence X-rays from electronic atoms. The fine pixel structure provides accurate determination of the X-ray line position while the excellent background rejection capabilities of the CCD, using both energy and topographical discrimination, are essential in the high background environment of a particle accelerator. © 2001 Elsevier Science B.V. All rights reserved.

## 1. Introduction

A series of recent and planned experiments at the Paul Scherrer Institut (PSI) makes use of characteristic X-rays from exotic atoms. Such atoms are formed when negatively charged particles like pions have been slowed down to a kinetic energy of a few eV by capture into the Coulomb field of atoms. The highly excited systems de-excite by the emission of electrons and X-radiation. For light exotic atoms formed in dilute targets the electron cloud is completely depleted by Auger emission, so that the exotic atom becomes a hydrogen-like system in which the energy levels can be calculated very precisely by the methods of bound-state QED, disregarding possible strong-interaction effects.

One aim of the present studies is to improve the accuracy of the pion mass from 3 to 1 ppm [1] by measuring the 5–4 transition in pionic nitrogen.

---

*Corresponding author. Tel.: +44-116-252-2007; fax: +44-116-252-2464.

*E-mail address:* nin@star.le.ac.uk (N. Nelms).

[1] Present address: WEY Elektronik AG, CH-8103 Untereng-stringen, Switzerland.

The energy of the transition gives the reduced mass of the system, from which the pion mass can be calculated. Another goal is a high-precision determination of the strong-interaction shift and broadening of the ground state in pionic hydrogen [2]. X-ray energies from transitions into the ground state are measured and, by comparison with QED calculations, the influence of the strong interaction is deduced.

For light exotic atoms, X-ray energies are in the few keV range, which require a reflection-type crystal spectrometer for ultimate energy resolution. Energy calibration is provided by X-rays from other exotic atoms, whose line widths are much narrower than those of normally used, fluorescence X-rays. A new experimental approach is to measure the line of interest simultaneously with the calibration line to reduce the chance of systematic errors. This major improvement from the previous measurement of the pion mass [3]

requires the large area CCD detector described here.

## 2. Detector requirements

The initial experiment for the new detector is a precise determination of the pion mass. Fig. 1 shows the experimental arrangement at the high-intensity pion beam line, πE5, of the PSI. Pions are injected into the cyclotron trap [4,5], where a weak-focussing magnetic field, produced by a superconducting split-coil, guides the particles in a spiral path to the centre of the trap. A vacuum chamber, situated in between the coils, contains an arrangement of radial foils and wedges for a fast degradation of the unstable pions. About 1% of the pions are stopped in a thin-walled cylindrical cell of 60 mm diameter, which is filled with the target gas. Muonic atoms are also formed,
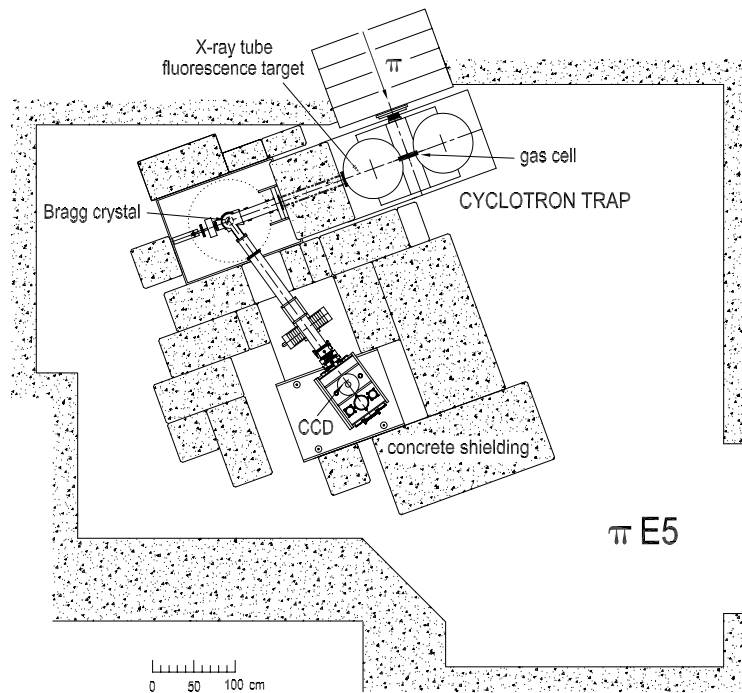


Fig. 1. Experimental arrangement for pion mass measurement, setup in the πE5 area at the PSI. Exotic atoms are formed inside the gas cell at the centre of the cyclotron trap. Emitted X-rays are energy analysed by Bragg reflection and recorded with the large area CCD detector, located at the focus of the spectrometer on the Rowland circle. Fluorescence X-rays used for set-up and calibration are generated by irradiating targets with an X-ray tube.

from the decay of slow pions close to the cell. A stop rate of only about 5% of the pion rate is achieved.

The energy measurement is performed with a Bragg spectrometer set up in Johann geometry. Using this geometry, all energies in a certain interval, given by the horizontal extension of the source, can be recorded simultaneously using a position-sensitive X-ray detector of corresponding size. This allows, in the case of the pion mass measurement, use of muonic transitions for energy calibration of the pionic spectral lines, since the muon mass is already known to 0.05 ppm [6].

Table 1 shows the transition energies and Bragg angles of the lines of interest. Copper fluorescence X-rays are used in the set up of the spectrometer. The muonic oxygen and pionic nitrogen lines differ by only $\sim 32$ eV or a change in Bragg angle of $\sim 36'$. With the Rowland circle radius of 1.5 m this corresponds to a line separation of $\sim 30$ mm at the detector or $\sim 1$ eV/mm. The simultaneous measurement of the two lines strongly reduces systematic uncertainties arising from possible mechanical or thermal instabilities of the spectrometer during long measurement periods. Use of a spherically bent crystal improves the count rate by partially focussing the lines in the vertical direction. In this way, about 80% of the reflection overlaps with the sensitive area of the detector described here, at Bragg angles around $53°$. The energy resolution of the crystal spectrometer achieved with a silicon crystal is $\sim 500$ and $\sim 700$ meV for 4 and 8 keV X-rays, respectively [7].

Table 1
Energies and corresponding Bragg angles of the measured lines[a]

| Transition | Energy (eV) | Bragg angle | Relative intensity (%) |
|---|---|---|---|
| $\pi^{-14}$N (5g–4f) | 4055.373 | $52°45'38.1''$ | 100 |
| $\mu^{-16}$O ($5g_{7/2}$–$4f_{5/2}$) | 4024.298 | $53°20'47.4''$ | 43 |
| $\mu^{-16}$O ($5g_{9/2}$–$4f_{7/2}$) | 4023.747 | $53°21'25.7''$ | 55 |
| $\mu^{-16}$O ($5g_{7/2}$–$4f_{7/2}$) | 4022.960 | $53°22'20.0''$ | 2 |
| Cu K$\alpha_1$ | 8047.83 | $53°32'44.4''$ | 66 |
| Cu K$\alpha_2$ | 8027.85 | $53°32'45.8''$ | 34 |

[a] The Bragg angles are for Si 220 reflection for exotic atom transitions and Si 440 for copper. Natural line width of exotic atom transitions is of the order of 10 meV [16]. Cu K$\alpha_1$/K$\alpha_2$ natural line width is 2.3 eV/3.3 eV [17].

For accurate determination of the line shape, good detector position resolution is essential together with adequate over-sampling (small pixel size). Two-dimensional position resolution is required to correct for the curvature of the reflection. The main energy of interest for the pion mass experiment is $\sim 4$ keV (Table 1). Because of the very low count rates (typically $< 100$ X-rays/h) the detector requires good quantum efficiency (QE) in this energy range. With the very high beam-induced background, just detecting the diagnostic X-rays alone is not enough, event discrimination and background reduction capabilities are mandatory. These are achieved by good energy resolution combined with high-position resolution. To meet all of these requirements, an array of X-ray sensitive CCDs were chosen as the detector.

## 3. Detector description and operation

### 3.1. CCD structure

X-ray sensitive CCDs for use in the 1–10 keV range have been developed for a number of X-ray astronomy missions, including JET-X [8] and XMM-Newton [9]. XMM-Newton carries three X-ray telescopes, two of which use a large area, X-ray sensitive CCD [10] developed jointly between the University of Leicester and Marconi Applied Technologies (formerly EEV). CCD22 devices from this program have been chosen as the focal detector of the crystal spectrometer. The CCD22 is a high-resistivity device, manufactured on 80 μm epitaxial silicon, with a depletion depth of $\sim 30$ μm and subsequently, a field-free region of order 50 μm. Each device has $600 \times 600$, 40 μm square pixels to make an imaging area of 24 mm $\times$ 24 mm. A simplified schematic is shown in Fig. 2. More detailed information can be found in Ref. [11].

The CCD22 has an open-electrode structure (Fig. 3) for low-energy response and employs high-resistivity silicon for high-energy response, which gives good QE over the range 0.2–10 keV. The QE for the main energy range of interest in the pion mass experiment, of order 4 keV, approaches 90% [11] (Fig. 4). The two output nodes are located at
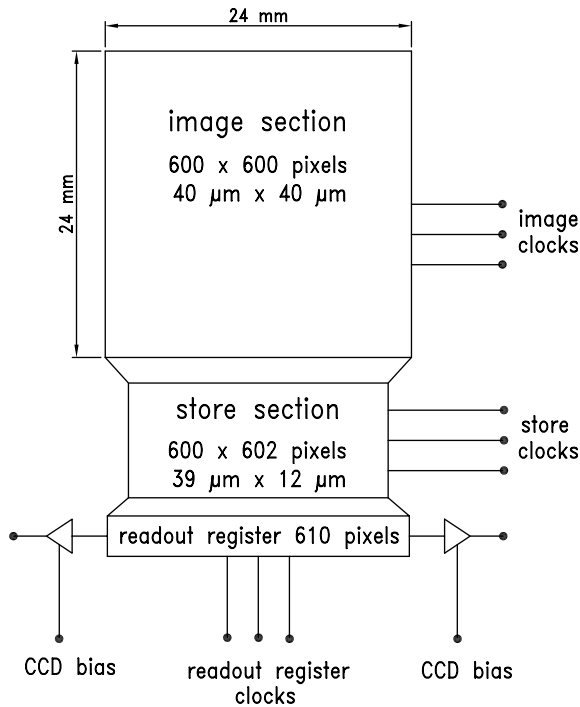
Fig. 2. Simplified schematic of CCD22 frame transfer device. The image section contains $600 \times 600$, $40\,\mu m$ square pixels. The store section has smaller pixels to reduce overall CCD size and allow devices to be butted together. The read-out register has 5 dark reference pixels at each end and with 2 extra rows in the store section, the final CCD read-out size is $610 \times 602$ pixels.

one end of the device and, using the CCD package developed for the XMM program, is three-sides buttable. The CCD22 is capable of operating in frame-transfer mode, where the image region can be rapidly shifted ($<20\,ms$) into a store region comprising an equal number of pixels, allowing image integration to continue during read-out. Thus, provided the integration period is greater than the read-out period, dead-time losses are eliminated.

### 3.2. Cryostat description

Each CCD22 is assembled on a thermally isolated package, with connection to a cold-finger for cooling. Electrical connection for clock and bias signals is provided through a kapton

flex-circuit. The six CCDs are mounted in a 2-column by 3-row array on a single, invar cold-finger (Fig. 5). This provides a total imaging area of $48\,mm \times 72\,mm$. There is a maximum gap of $500\,\mu m$ between CCDs and they are rotationally aligned to better than 7 mrad. The whole assembly is housed inside a custom built stainless steel vacuum cryostat (Fig. 6). The cold-finger is cooled using liquid nitrogen and closed loop control maintains a CCD temperature of $-100 \pm 0.5°C$, which reduces the thermally generated "dark current" to negligible levels. The CCD array is wrapped in $5\,\mu m$ metallised mylar, cooled very quickly by direct connection to the liquid nitrogen feed. This acts to condense any remaining water or contaminants before the CCD surface has cooled. A gate valve allows disconnection of the spectrometer tube without losing cryostat vacuum. The electronic boxes for temperature control and CCD drive are mounted on top of the cryostat behind the liquid nitrogen dewar.

The cold-finger is mounted (thermally isolated) on a motorised, high-precision translation table which gives control over the distance of the CCD array to the Bragg crystal. Remote adjustment over a range of 95 mm is possible, to match the focal length of the crystal in use. The position perpendicular to the crystal-detector direction (transverse offset), i.e. the direction of dispersion, is controlled by a precision gauge and is reproducible to $1\,\mu m$. The vertical direction is fixed. Movement of the linear table, verification of the transverse offset, and measurement of various temperatures of the $LN_2$ cooling system with PT100 resistors, were all included in the crystal spectrometer control.

The entrance aperture comprises of a $5\,\mu m$ aluminised, Mylar window and is protected against over-pressure by an automatic by-pass arrangement which is closed when the spectrometer vacuum is above $10^{-3}\,mbar$. Below this pressure, the gate valve can be opened in front of the CCD allowing for measurement of X-rays reflected from the crystal. The spectrometer vacuum is controlled by a safety circuit, which isolates the cryostat vacuum in the case of a spectrometer vacuum failure by closing the gate valve and opening the window bypass.
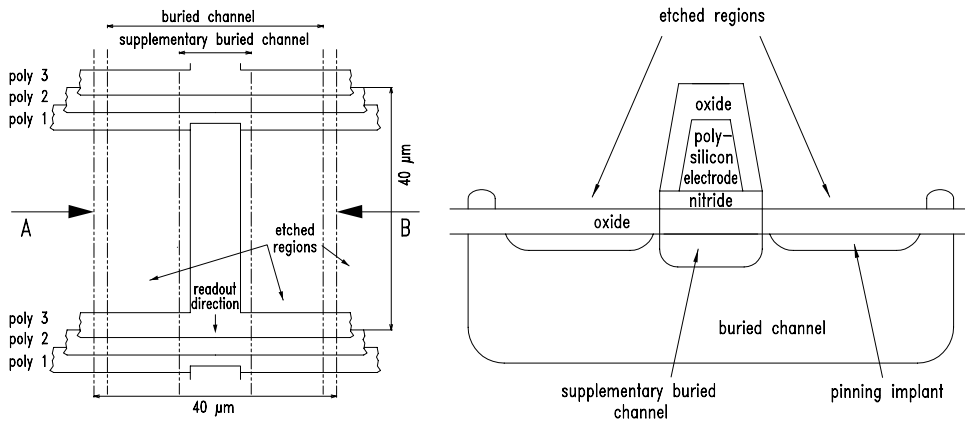
Fig. 3. CCD22 pixel schematic and enlarged cross-section view through A-B. The etched (open) regions in the enlarged poly-silicon electrode (Poly 3) reduce absorption in the overlying electrode structure, improving low-energy X-ray quantum efficiency.
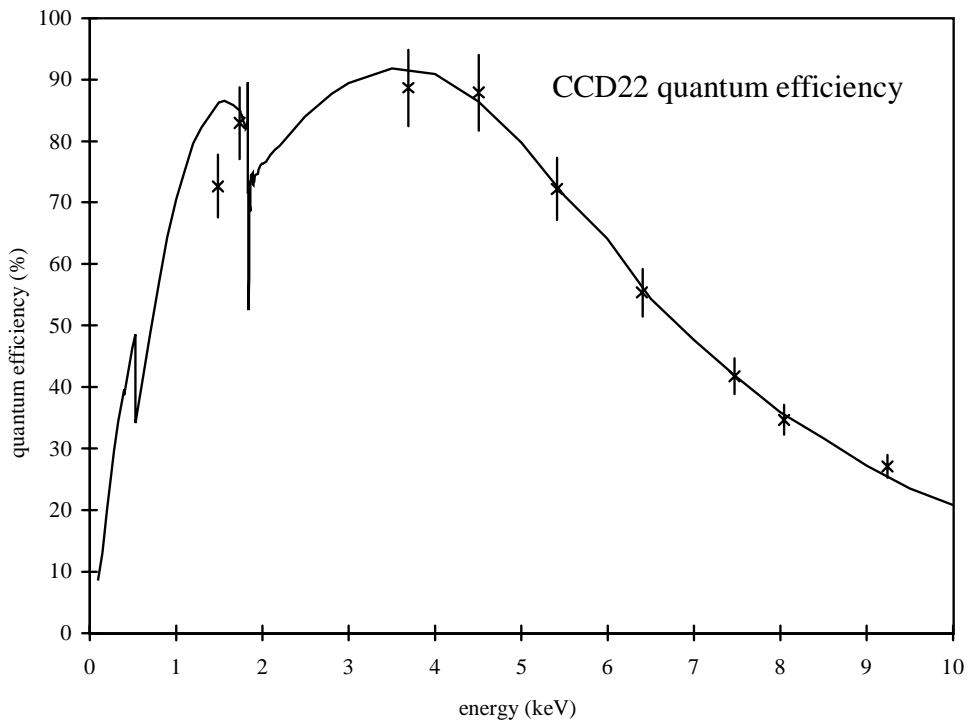
Fig. 4. CCD22 quantum efficiency measured at Leicester University [11]. The solid line is a simple analytical model using the absorption depth of photons in silicon combined with absorption in the overlying electrode structure and associated layers.

An $^{55}$Fe calibration source is used to determine and control energy calibration and resolution at 5.9 keV during the measuring periods.

### 3.3. Detector operation

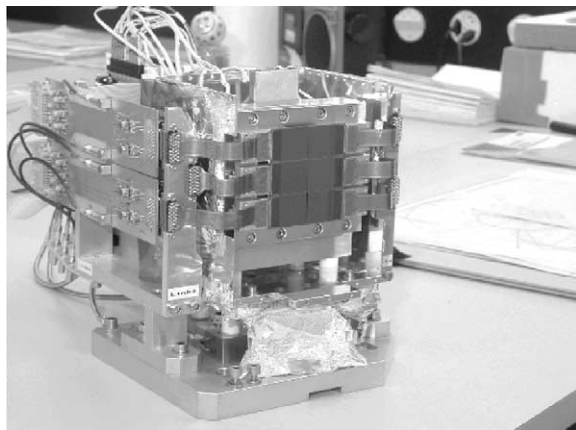Precise energy cuts and efficient background rejection require low noise operation of the CCDs

Fig. 5. Photograph showing $2 \times 3$ CCD array mounted on cold-finger, prior to installation inside vacuum cryostat. Total imaging area is $48 \, mm \times 72 \, mm$.
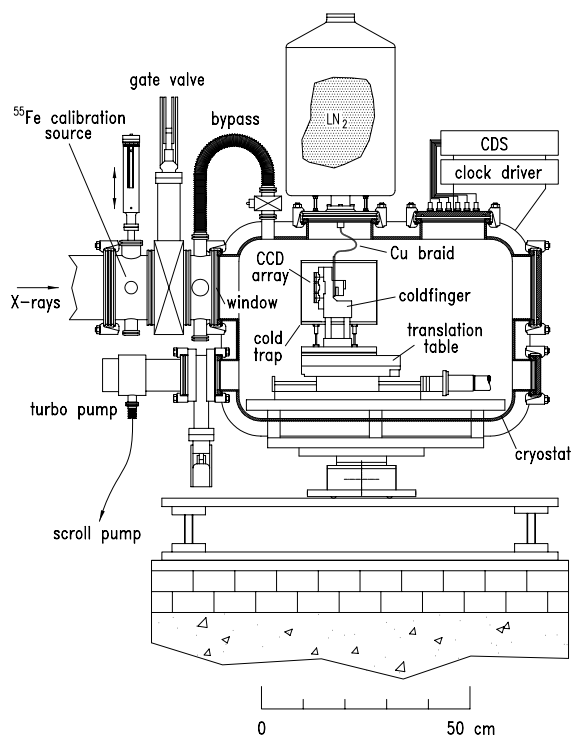


Fig. 6. CCD cryostat detail.

and are necessary to enable the X-ray emission line profiles to be measured accurately. The dominant noise sources in slow-scan CCD operation are thermally generated dark current and reset-noise

fluctuation [12]. At $20°C$, typical dark current generation is of order $10\,000–30\,000$ electrons/pixel/s. This causes two problems. Firstly, full-well capacity may only be $100\,000$ electrons and so the pixel can saturate after only a few seconds. Secondly, the noise contribution is poissonian and so 1 s of dark current generation can add (in quadrature) 170 electrons rms to the read-noise. Cooling the CCDs to $-100°C$ reduces thermal charge ($Q_t$) generation in the silicon to $<10$ electrons//pixel/h. The effective noise contribution from the thermal charge ($Q_t^{1/2}$) can now be neglected. CCD operation typically comprises resetting of the output node prior to sampling of the pixel charge. Once cooled, the read-noise becomes dominated by the variation in the DC level achieved after each reset. This variation, typically a few hundred electrons, can be effectively removed by a technique known as correlated double sampling (CDS) [13,14]. In this method, the output of the CCD is sampled twice for every pixel. First, the CCD output is reset and the DC level sampled. Second, the CCD pixel charge is clocked onto the output node and also sampled. The two samples are then correlated (subtracted) to provide a reset-variation free measurement of the pixel charge. This technique can be performed in several ways, both in the analogue and digital domains. Analogue methods include clamp-and-sample and dual slope integration. Digital double sampling relies upon digitisation of the reset level and the charge level which are then subtracted digitally. We have chosen a dual slope integration technique, where both the reset level and the charge level are integrated and then subtracted, since the integration operation provides additional low-pass filtering to improve the noise performance further.

The six CCD22 devices are controlled from an IBM compatible PC using a combination of custom and commercial electronics (Fig. 7). Two PC expansion cards supply software programmable bias voltages and clock sequences. These signals are then multiplexed in the Clock Driver box to drive one column of CCDs each. Read-out of the two columns is synchronised, such that the frame transfer of all six CCDs occurs simultaneously. Once a frame transfer has been
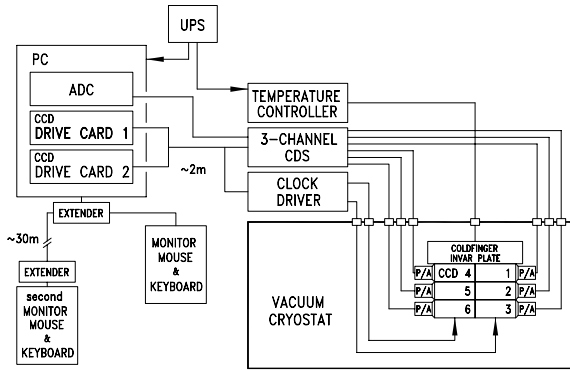
Fig. 7. CCD drive electronics. An un-interruptible power supply (UPS) is used to supply the CCD control PC. Extender boxes allow the keyboard, monitor and mouse to be located up to 30 m away from the PC base unit, outside the experimental area.

performed, the storage regions of the left CCD column are read out, followed by the right. A 3-channel CDS amplifier is multiplexed between the two columns of CCDs. A 12-bit, multi-channel PC ADC card digitises the outputs from the dual-slope integrator. Bias voltage and clock voltage levels, integration time, on-chip binning and timing parameters are all adjusted via software control.

Long integration times ($>1$ h) are possible with cryogenic operation of the CCDs, without thermal charge contributing to the background signal. However, in the high background environment of the pion beam line at PSI, background events at a rate of 20 000/CCD/h have been recorded. A pixel activated by a background particle from the beam line is either saturated or holds an indeterminate amount of charge and is unable to detect an X-ray. The X-ray count rate at the CCD in some cases is as low as 15–20/h and any detector area lost through background activation is undesirable. Two methods of operation are used to minimise these losses. The frame rate is operated at (near) maximum which reduces the number of beam-line generated background effects, per frame, to a minimum. Frame transfer operation, with its effective zero dead-time, maximises the X-ray detection rate in each frame. After frame transfer, read-out of the whole CCD array takes $\sim 30$ s. In frame transfer mode, the image area of

the CCD is integrating while the storage region is read out, so the minimum integration time is $>30$ s, equal to the read-out time of the CCD. In practice, an overall integration time of 1 min was used.

Minimising the integration time maximises the frame rate and has an impact on the quantity of data generated. Each CCD has $600 \times 600 = 360\,000$ pixels, digitised to 12-bits. Assuming two bytes per pixel, one full image from six CCDs would amount to 4.3 Mb, corresponding to 6.2 Gb of data per day (at 1 frame/min). Back-up and transfer of this quantity of data over a ten-week beam run time is difficult and real-time data compression is required. The calibration of each CCD enables the read-noise peak position and standard deviation to be determined. From this, a noise threshold (peak position plus 3- or 5-standard deviations) is calculated and only active CCD pixel signals, with a value greater than threshold, are stored (thresholded data). Processing is done after each frame of CCD data has been read into the PC. For each active pixel, five bytes are used: three for position and two for energy. In comparison to raw data storage (360 000 pixels), there may be only 2000 active pixels per minute for a full six-CCD image, mostly containing background events. This reduces the data rate to 600 kb/h or $<15$ Mb/day, a factor of $>400$ reduction on the raw data rate.

## 4. Results

### 4.1. CCD evaluation and laboratory measurements

Eight CCD22 devices, two of setup and six of scientific grade, were purchased and assembled onto XMM flight packages. Each device was tested individually, under vacuum at $-100^{\circ}$C, using titanium X-rays fluoresced by an $^{55}$Fe source. Image quality or cosmetic appearance, read-noise and charge transfer efficiency (CTE) were all evaluated and operating voltages and timing parameters were optimised. Three CCDs were then assembled together and driven in parallel by one set of bias-clock voltages from a single computer control card. These voltages were

selected to give the best overall performance of the three devices. This process was repeated for both sets of 3-CCD arrays.

As expected, only the two set-up grade devices exhibited cosmetic defects, in the form of bright columns, created by the charge generated in a "hot" pixel which floods the column during frame transfer or read-out. All the scientific grade devices were free of column defects. Since the CCD array is not used for imaging, the bright columns result only in a small reduction of the collecting area (1/600 of a CCD per bright column). Of the first six CCDs delivered, one was a set-up grade. Due to beam run schedule constraints and otherwise good quality of the set-up grade device, all of the first six devices were fitted onto the CCD array cold-finger assembly. This is not a simple task and so it was decided not to exchange the set-up grade CCD, once the two remaining devices became available. Table 2 lists the noise performance of the six CCDs in the detector array. Read-noise was never greater than 6 electrons rms with a calibration of $\sim 1.6$ eV/ADC channel for laboratory conditions.

The spectra in Fig. 8 are the summed results of fifty frames of thresholded CCD data, using a 10 s integration period. They were all taken using titanium X-rays (4.51 keV). The top plot shows an energy histogram of all active CCD pixels. Multiple pixel events, where the charge generated by a single X-ray photon is spread over several pixels, appear in the spectrum between the areas indicated. In the middle plot, only isolated CCD events are shown. The area below the titanium Kα peak is now much cleaner with the spread event charge removed. The bottom plot shows the same spectrum but with the vertical scale expanded. The
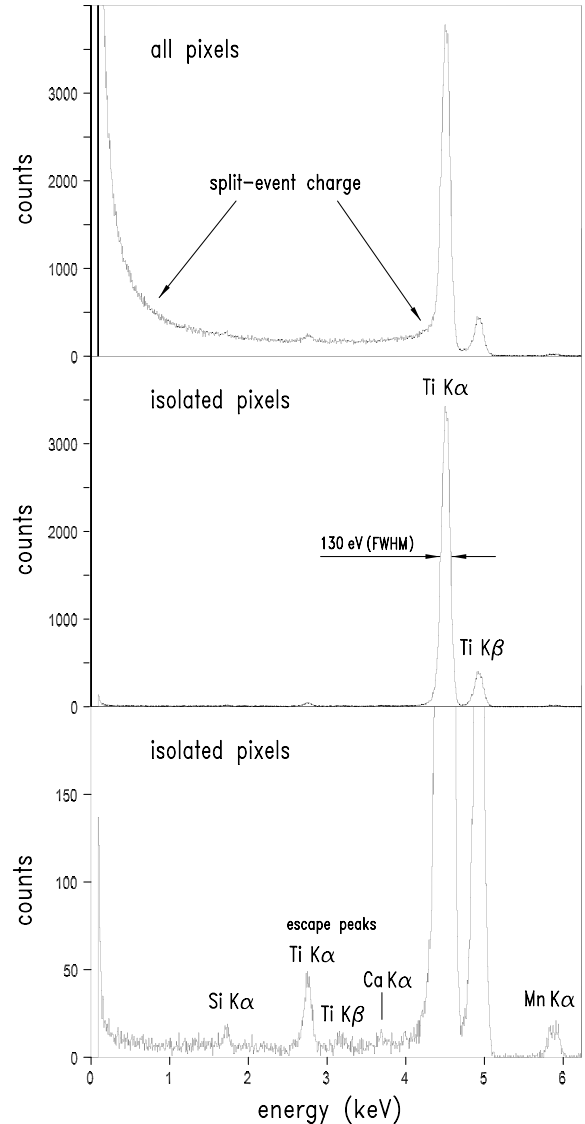


Fig. 8. CCD energy spectrum taken with titanium fluorescence X-rays. The top plot shows raw CCD data. Cluster analysis to remove all multi-pixel events produces the clean spectra in the middle which, in the bottom plot, has been expanded in the vertical direction.

titanium escape peaks are now clearly visible along with the associated silicon K (1.73 keV) line. Manganese Kα (5.9 keV) is from the $^{55}$Fe source directly whilst the aluminium (1.49 keV) is from the $^{55}$Fe source mount or part of the laboratory cryostat. The line at 3.7 keV is probably calcium,

Table 2
Laboratory measured CCD parameters

| CCD | Read noise (el rms) | FWHM at Ti Kα (eV) |
|---|---|---|
| 1 | 4.88 | 148 |
| 2 | 5.00 | 130 |
| 3 | 5.01 | 136 |
| 4 | 4.76 | 130 |
| 5 | 5.59 | 132 |
| 6 | 4.81 | 130 |

from a separate target on the target wheel. The full width half maximum (FWHM) of the titanium peak is typically 130 eV (Table 2), while at manganese (5.9 keV) it is typically 150 eV.

## 4.2. CCD alignment

Reflected spectra cover a single column of CCDs with reflections on both columns and so correct determination of the peak position and separation requires accurate knowledge of relative CCD rotation and displacement. To provide the relative location and orientation information for each CCD, a remote controlled, motorised aluminium mask, with identifying features, is positioned in front of the detector array. The alignment measurement was done by illuminating the CCD array through the mask using sulphur (2.3 keV) fluorescence X-rays excited by means of an X-ray tube. To avoid aberrations, the sulphur target was positioned ~3.3 m in front of the mask, which in turn is ~35 mm from the CCD array. A 5 mm diameter collimator was placed 10 cm in front of the sulphur target, to produce an approximate "point like" source and to eliminate unwanted scatter. CCD data was collected for 60 h (~660 000 events) and is illustrated in Fig. 9.

The mask is arranged to provide either a horizontal or vertical line and a diagonal line, which cross the boundary between adjacent CCDs. Using this pattern, determination of the alignment is possible without precise knowledge of the distance between the mask and CCD surface. A least-squares fit is used to obtain the slope of the lines on each CCD and corrections are determined for the relative rotation about the centre of each device. After rotation has been corrected, a new line fit is performed to determine the boundary intercept and offset between adjacent CCDs. The CCDs are numbered from 1 to 6 with the right-hand column containing devices 1 to 3 and the left-hand column, devices 4 to 6, when viewed from the crystal. CCDs 1 and 4 are at the top. Table 3 lists the measured rotations and offsets relative to CCD 3 (bottom right). The errors are statistically limited, by the number of events in the alignment image. The mask pattern is very precisely cut, with
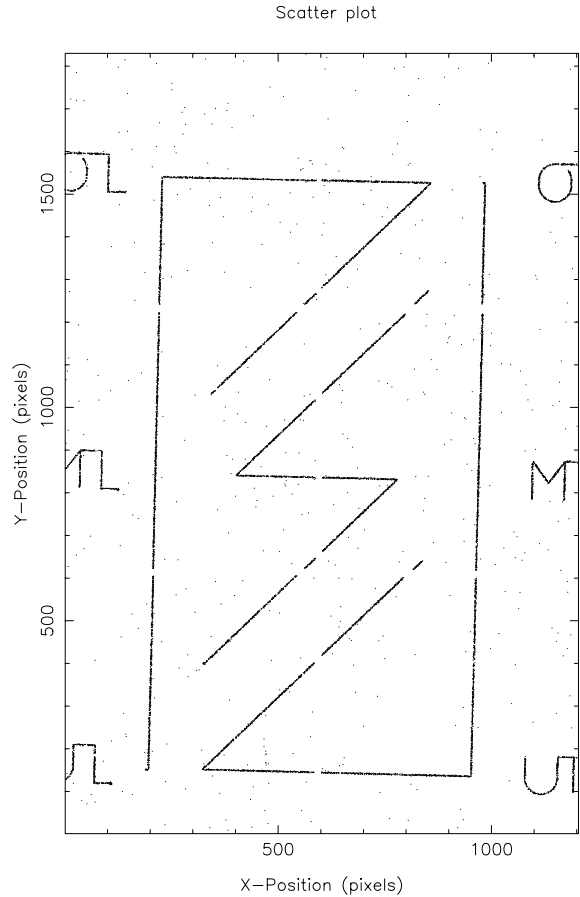


Fig. 9. CCD image plot showing alignment mask detail as measured with suphur fluorescence X-rays (front view). The mask image contains ~600 000 events. CCD boundaries are at 610 and 1220 in the Y-position direction and 602 in the X-position direction.

Table 3
Measured CCD alignment corrections[a]

| CCD | Rotation (mrad) | Horizontal disp. (pixels) | Vertical disp. (pixels) |
|---|---|---|---|
| 1 | 0 ± 0.2 | −2.57 ± 0.07 | 22.31 ± 0.22 |
| 2 | 0.3 ± 0.2 | −0.98 ± 0.04 | 10.88 ± 0.16 |
| 4 | 1.7 ± 0.3 | −14.93 ± 0.13 | 20.35 ± 0.23 |
| 5 | 2.8 ± 0.3 | −15.29 ± 0.11 | 11.69 ± 0.17 |
| 6 | 6.5 ± 0.2 | −17.13 ± 0.10 | 0.59 ± 0.05 |

[a] Rotations (positive corresponds to an anti-clockwise rotation) and displacements are relative to CCD3 (see text and Fig. 9).

a width of 150 μm and an integral non-linearity of 5 μm from top to bottom.

### 4.3. Results from measurements at the pion beam line

Two beam runs, set up as in Fig. 1, have taken place in the πE5 area at PSI, with the aim of a new determination of the charged pion mass. X-rays from the 5g–4f transition of muonic oxygen are focussed on to the left-hand column of CCDs, for calibration, while X-rays from the 5g–4f transition of pionic nitrogen are focussed on to the right. At regular intervals, Cu Kα fluorescence X-rays were measured as a stability and calibration check. Typically, a 1 min integration period was used and thresholded data recorded in multiples of 60 frames.

Fig. 10 shows energy spectra and two-dimensional position distributions which demonstrate the difference with and without beam conditions. The copper X-rays were generated using an X-ray tube and a fluorescence target without beam in the area and hence are practically background free. The energy spectrum is taken from a single CCD and shows the reflected Cu Kα line at 8.047 keV, reflected in fourth order by a silicon crystal cut along the (1 1 0) plane. The low energy side of the spectrum has been expanded in the vertical direction to show a number of direct interaction lines. Aluminium is from the CCD cold-trap. A few X-rays from a scandium target, mounted close to the copper target are seen, because the Bragg angle in second order is close to that for copper in fourth order. Chromium is from the casing of the mask motor whilst the line at 6.31 keV is the copper Kα escape peak associated with the silicon line at 1.73 keV. On the reflection plot the Kα$_1$ and the Kα$_2$ lines, separated by 20 eV, are clearly resolved. The gap between the columns of CCDs can be seen in the centre of the plot. For higher energy X-rays, above ∼6 keV, the attenuation length in silicon results in a significant proportion (∼70% for Cu K) of the photons being absorbed below the CCD depletion depth (∼30 μm), in the field-free region. Consequently, charge spreading occurs much more readily [15] and results in a large increase in the number of multi-pixel events

(Fig. 11). With a focussing spectrometer photons may be concentrated onto a small area of the CCD. Unless care is taken to adjust the count rate, the spectral and positional information contained in the depletion region absorbed X-rays (generally 1–2 pixels) may be destroyed, by losing the isolation that surrounds these events. In the case of Cu K, the average size of event for a photon absorbed in the field-free region has been measured as 9 pixels. With only 30% of X-rays absorbed within the depletion depth, a ratio of 16:1 field-free to depletion region active pixels is generated. As an example, 100 incident X-ray photons could result in the creation of typically 640 active pixels containing split charge generated in the field-free region and only 40 active pixels from the depletion region absorbed events. Since the Cu Kα$_1$ reflection is only of order 25 pixels wide (FWHM), and allowing only 2% of pixels to be activated, the incident X-ray rate needs to be <2 photons/s when using a 1 min frame integration time. This is typically an order of magnitude reduction over count rates possible with lower energy X-rays. On a further note, it may be possible to improve the resolution of the reflected line over that given by the intrinsic pixel size of the CCD, by detailed examination of spread-events collected from the field-free region. A multi-pixel event can be identified as coming from a single photon using energy and topographic discrimination. It is then possible to determine the centroid of the event on an energy basis and obtain a sub-pixel location for the original interaction position of the photon.

The remaining plots in Fig. 10 show X-rays from pionic nitrogen (πN) and muonic oxygen (μO) (5–4) transitions recorded simultaneously, over a 50 h period. An approximately equal count rate for both the πN and μO lines was achieved by using an N$_2$/O$_2$ mixture of 10%/90%. The middle plots show the raw data with no background subtraction applied. The X-ray lines are indistinguishable in the energy spectrum. In the image plot, only data from a short period of time is shown, otherwise the image would be completely black. A cosmic ray track, which crosses the boundary between two adjacent CCDs, is visible in the upper left. Fast, charged particles or high-
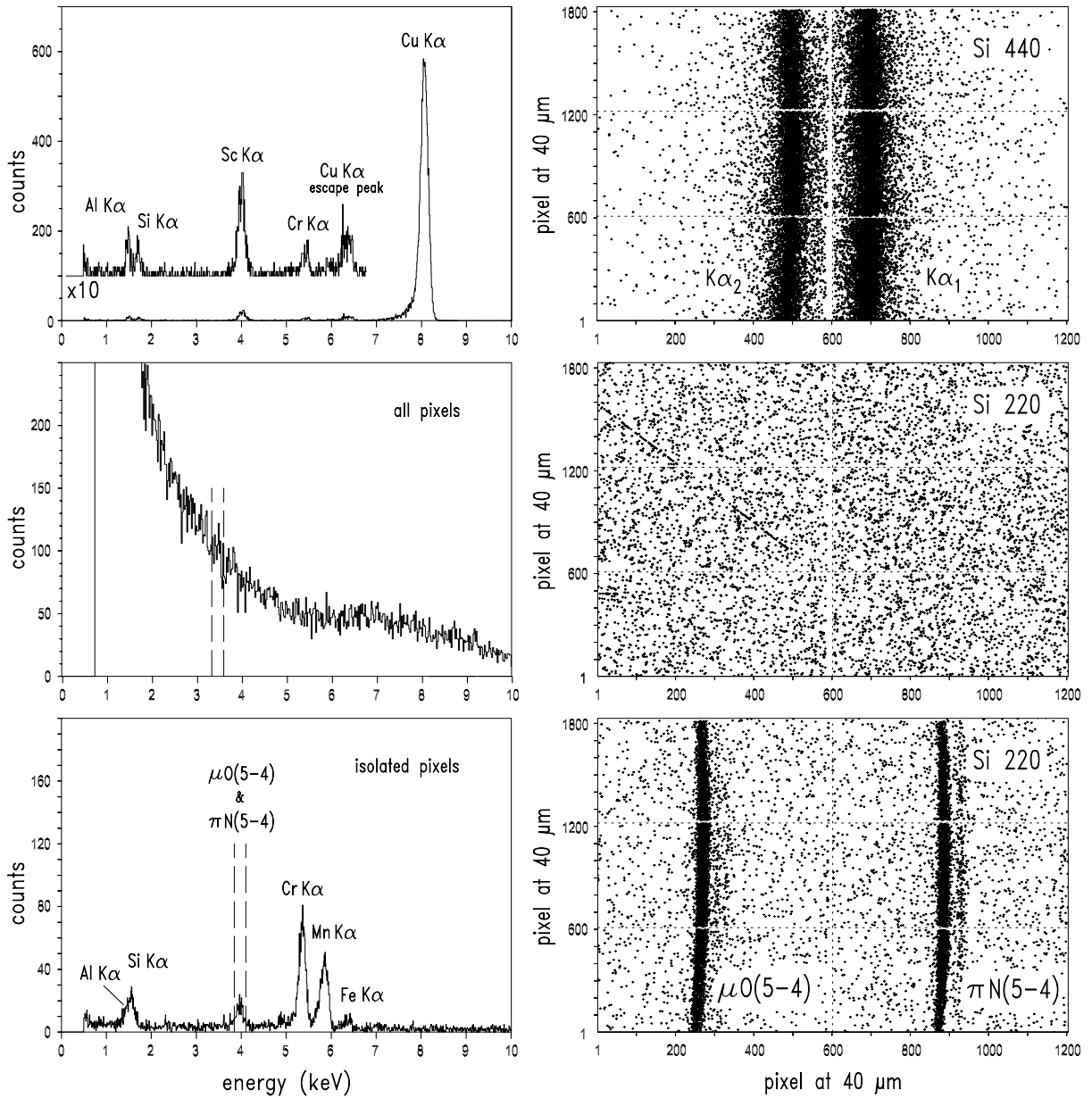
Fig. 10. Energy and two-dimensional position spectra of X-rays from Cu Kα fluorescence (top). Simultaneously recorded πN and μO (5g–4f) transitions are shown before cluster analysis (middle) and after (bottom) demonstrating effective background subtraction. The low-intensity lines on the high-energy side are the parallel transitions (5f–4d).

energy Compton-induced events generally create multi-pixel events in the CCD, whereas for low energy X-rays, the charge is generated by photo-effect and, if the interaction occurs within the depletion region, typically deposited in one or two adjacent pixels only. At 4 keV, the energy of the pionic and muonic lines, ~90% of X-rays are converted before reaching the field-free region. Applying energy and topographic discrimination, an improvement in the signal-to-noise ratio by
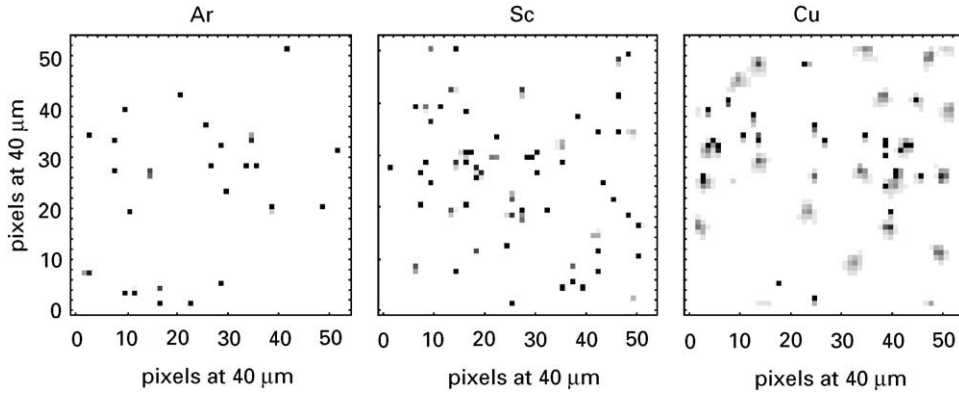
Fig. 11. Comparison of event cluster size for incident X-rays of 2.96 keV (Ar), 4.10 keV (Sc) and 8.04 keV (Cu). Each plot shows a 50 pixel square region from the centre of the reflection. The large increase in multi-pixel events for Cu X-rays is evident, due to conversion in the field-free region of the CCD.

Table 4
Comparison of event data for beam on and off conditions[a]

| X-ray | Energy (keV) | No. hit pixels in energy cut | | | X-ray source |
|---|---|---|---|---|---|
| | | No. cluster analysis | 1 pixel events | 2 pixel events | |
| πC (5g–4f) | 2.97 | 1692 | 11 | 5 | Pion beam |
| Ar Kα | 2.96 | 11466 | 10077 | 3042 | X-ray tube |
| πN (5g–4f) | 4.06 | 274 | 16 | 6 | Pion beam |
| Sc Kα | 4.09 | 45662 | 25984 | 9467 | X-ray tube |

[a] Data is for $10^5$ hit pixels ( $> 5\sigma$ above the noise peak). Very high background during beam is effectively removed using energy and topographical discrimination.

several orders of magnitude is achieved. X-ray lines in the energy spectrum (Fig. 10 bottom) are now prominent with the πN and μO (5–4) reflections clearly defined in the image plot. Table 4 illustrates event data collected using different sources under beam and no beam conditions. Removal of the very high background generated with beam on is effectively demonstrated by comparing the number of hit pixels with the actual data recovered once energy cuts and cluster analysis has been applied.

From the two-dimensional image plot, the curvature of the reflections is apparent. By applying curvature correction, which is easily obtained from the two-dimensional position information, and binning the image data in the vertical direction we obtain the position spectra in

Fig. 12. Correction for individual CCD displacement in the vertical and horizontal directions has also been applied. In the πN and μO plot, the 5g–4f transitions are well defined with the smaller, parallel 5f–4d transitions appearing. The peak-background ratio of the 5g–4f transitions is of order 60:1, even with very low count rates of $\sim 15$/h.

## 5. Conclusion

We have designed and built a large-area, CCD detector system (48 mm × 72 mm) for measuring X-ray lines at the focus of a Bragg reflection spectrometer. The high-resitivity CCDs have good detection efficiency and excellent background
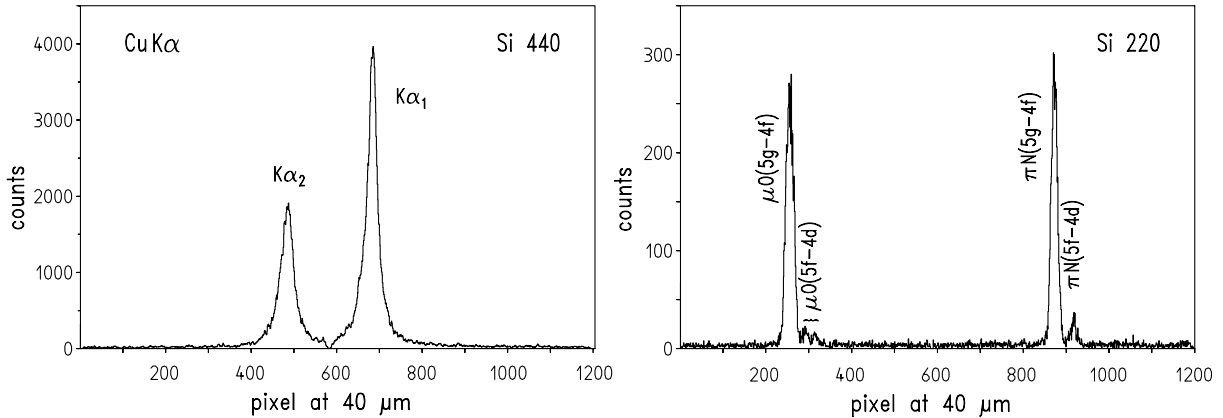
Fig. 12. Position spectra for reflections from Cu Kα (left) and simultaneously recorded πN and μO (5–4) transitions. The two-dimensional image was corrected for curvature of the reflection before projecting onto the axis of dispersion. The fine-structure of the μO (5g–4f) transition is not resolved (see Table 1).

rejection capabilities. Stable, low noise operation has been demonstrated under beam conditions and over long runs. Using intensive post-processing of the collected data, along with the careful application of a large quantity of concrete shielding, the overwhelming neutron-induced background in the vicinity of the beam-line has been counteracted.

## References

[1] PSI prop. R-97.02 (1997).
[2] PSI prop. R-98.01 (1998) (http://pihydrogen.web.psi.ch).
[3] S. Lenz, G. Borchert, H. Gorke, D. Gotta, T. Siems, D.F. Anagnostopoulos, M. Augsburger, D. Chatellard, J.P. Egger, D. Belmiloud, P. El-Khoury, P. Indelicato, M. Daum, P. Hauser, K. Kirch, L.M. Simons, Phys. Lett. B 416 (1998) 50.
[4] L.M. Simons, Phys. Scr. T22 (1988) 90.
[5] L.M. Simons, Hyperfine Interactions 81 (1993) 253.
[6] D.E. Groom, et al., (PDG), : Eur. Phys. J. C 15 (2000) 1.
[7] T. Siems, D.F. Anagnostopoulos, M. Augsburger, G. Borchert, D. Chatellard, J.P. Egger, P. El-Khoury, D. Gotta, P. Hauser, P. Indelicato, K. Kirch, L.M. Simons, Phys. Rev. Lett. 84 (2000) 4573.
[8] A.A. Wells, D.H. Lumb, K.A. Pounds, G.C. Stewart, B. Aschenbach, H. Brauninger, G. Hasinger, J. Trumper, O. Citterio, L. Scarsi, A. Peacock, B. Taylor, Proc. IAU Coll. 115 (1990) 318.
[9] D.H. Lumb, H. Eggel, R. Laine, A. Peacock, Proc. SPIE 2808 (1996) 326.
[10] A.D. Holland, M.J.L. Turner, A.F. Abbey, P. Pool, Proc. SPIE 2808 (1996) 414.
[11] A.D. Short, A. Keay, M.J.L. Turner, Proc. SPIE 3445 (1998) 13.
[12] A.D. Holland, Ph.D. Thesis, Leicester University, 1990, p. 40.
[13] G.R. Hopkinson, D.H. Lumb, J. Phys. E 15 (1982) 1214.
[14] R. Kansy, IEEE J. Solid-State Circuits SC-15 (1980) 373.
[15] K.J. McCarthy, A. Owens, A.D. Holland, A. Wells, Nucl. Instr. and Meth. A 362 (1995) 538.
[16] S. Boucard, P. Indelicato, 1998, private communication.
[17] G. Hölzer, M. Fritsch, M. Deutsch, J. Härtwig, E. Förster, Phys. Rev. A 56 (1997) 4554.